Dean Vortices in Curved Tube Flow: 5. 3-D MRI and Numerical Analysis of the Velocity Field

Kun Yong Chung and Georges Belfort
Bioseparations Research Center, Dept. of Chemical Engineering, Rensselaer Polytechnic Institute, Troy, NY 12180

William A. Edelstein
GE Corporate Research & Development, Schenectady, NY 12301

Xianming Li
Fluent Inc., Lebanon, NH 03766

The velocity contour profiles within Dean vortices produced by flowing water in a solid-walled curved tube are quantitatively measured. Magnetic resonance flow imaging using flow encoding with spin warp imaging is used in two and three dimensions to obtain these velocities. These experimental measurements are then compared with simulations obtained from solutions of the Navier-Stokes and continuity equations for three axial flow rates. Numerical solutions were obtained with a finite volume method for curved tube Poiseuille flow.

Introduction

Concentration polarization (solute buildup at the solution-membrane interface) and membrane fouling are limiting phenomena that need to be controlled for improved membrane filtration performance. Methods to increase migration of solute from the region of the membrane surface to the cross-flowing bulk solution include the use of very fast flows (turbulence), the placement of inserts in the channel and/or on the membrane surface. All of these methods increase axial pressure drop substantially over laminar flow without these inserts. Recent work has shown that fluid instabilities such as Taylor vortices are extremely effective in depolarizing solute buildup and in shearing cake-type fouling off the membrane surface (Kroner et al., 1987). Unfortunately, annular flow filtration has serious limitations including the difficulty to scale up the size of the filter and to seal the system and prevent leakages. We have developed a new method based on Dean vortex formation resulting from flow in a curved duct that overcomes the limitations of scaleup and of sealing and does not exhibit inordinate pressure losses in the axial direction.

The results presented here are part of a comprehensive effort to study the behavior of Dean vortices in prescribed curved ducts using sophisticated analytical and numerical techniques together with optical and magnetic resonance flow imaging (MRFI) methods (Chung et al., 1992a,b,c). Eventually, we plan to use this know-how for developing a new membrane module in which Dean vortices will depolarize the buildup of dissolved and suspended solutes at the membrane surface interface (Belfort et al., 1992). Although we have used optical methods to *qualitatively* confirm the presence of the Dean vortices (Chung et al., 1992c), in this article, we report on the use of MRFI to *quantitatively* measure their velocity contour profiles within vortices. As a first attempt, we chose to study flow instabilities in a solid-walled 180° curved tube. The purpose of this study was to (i) refine the MRI methods (develop pulse sequences for both two- and three-dimensional flow patterns and their calibration curves), and (ii) determine their resolution and accuracy for measuring vortex contour velocities by comparing the MRI results with those from Olsen and Snyder (1985) and our numerical analysis using a finite volume technique. Additionally, once these methods have been developed, they will be used to determine the existence, persistence and strength of the vortices with axial distance (along a straight path following a slit curve) and axial flow rate (Chung et al., 1993d).

Here, we investigate three-dimensional velocity profiles for flow in a curved, circular cross-section tube using a numerical finite volume method (Patankar, 1980) and experimentally by nuclear magnetic resonance imaging (NMRI). In this design, at high enough flow rates steady laminar flow changes to unstable viscous flow resulting in rotating spiral vortices (often

Correspondence concerning this article should be addressed to G. Belfort.
Present address of K. Y. Chung: Korea Institute of Science & Technology, P.O. Box 131, Cheongryang, Seoul, Korea.

called Dean vortices). The objective is to measure noninvasively the mean velocity profiles (or velocity contours) in these vortices.

Centrifugal instability in the form of toroidal vortices can occur when a viscous fluid flows in a curved duct owing to a pressure gradient acting round the duct (Dean, 1928; Drazin and Reid, 1981). As with the Taylor vortex problem, both the wide-gap (Walowit et al., 1964) and the narrow gap approximation (Hammerlin, 1958; Reid, 1958) cases have been studied. Laminar developing curved-pipe flows have been investigated by numerous researches (see review by Berger et al., 1983). Also, numerical calculations of experimental flows (Patankar et al., 1974; Soh and Berger, 1984; Humphrey et al., 1985; So et al., 1991; Lai et al., 1991) and oscillitary flows (Eckmann and Grotberg, 1988) have been performed.

Experimental studies of flows through 90° and 180° bends have used one of two techniques (Olson, 1971; Agrawal et al., 1978; Choi et al., 1979; Enayet et al., 1982; Akiyama et al., 1983; Olson and Snyder, 1985; Bovendeerd et al., 1987; Ligrani and Niver, 1988; Takami et al., 1990; Bottaro et al., 1991). Both techniques have their problems. The laser Doppler velocity (LDV) approach is noninvasive, but has serious sensitivity limitations near walls; according to Bradshaw (1987), it cannot be relied upon to produce accurate cross-stream flow statistics for turbulent flows. The hot wire technique is invasive and could effect the secondary flows and hence the measurement of the vortices. In this work, we will introduce for the first time a relatively new technique, magnetic resonance flow imaging, for measuring vortices.

The first report measuring flow by NMR was probably by Suryan (1951) who showed that when partially saturated spins were replaced by unsaturated flowing spins, the continuous wave NMR signal intensity increased. This principle was used by Singer (1959) to demonstrate *in-vivo* flow measurement. There have been several reviews of NMR and flow, including those by Jones and Child (1976), Singer (1978), Battocletti et al. (1981), and Hemminga (1984). Recently, Caprihan and Fukushima (1990) reviewed the literature on liquid flow velocity measurements by pulsed NMR. Callaghan and Xia (1991) applied a pulsed gradient spin echo method at high spatial resolution and demonstrated the possibility of obtaining velocity and diffusion maps for water in laminar capillary flow. Heath et al. (1990) and Hammer et al. (1990) measured the fluid velocity profile in the extracapillary space of a hollow-fiber bioreactor. Agreement between these longitudinal flow velocity measurements in the capillary of a single hollow-fiber module and predicted longitudinal velocity contour plots was good. Kose (1990, 1991, 1992) has reported on the use of echo planar imaging (EPI) for studying turbulent flow. Pangrle et al. (1992) investigated the steady, laminar, incompressible fluid flow in a porous tube and shell system by using a time of flight (TOF) technique. Xia et al. (1992) have measured the velocity profiles through an abrupt contraction and expansion. Despite its enormous potential, NMR has not been used widely for flow measurements until recently. Cost, specialized know-how, and lack of sensitivity are probably the reasons for this. An important advantage of NMR is that it is noninvasive. Most NMR flow experiments, however, measure an average flow property over time, in contrast to methods like laser Doppler and hot wire which can measure instantaneous values of velocity. Thus, NMR is more appropriate for measuring steady-state flows or those in which the average behavior changes relatively slowly.

After presenting details of the theoretical method, we discuss the flow system, the NMR system and protocol, and measurements of the two- and three-dimensional pulse sequences with flow calibration. Then, the longitudinal and transverse velocities are discussed.

Theoretical Studies

The governing partial differential equations for a laminar flow in a three-dimensional geometry are solved numerically with the finite control volume method (Patankar, 1980). With this method, the computational space is divided into small control volumes. Within each of these control volumes, mass and momentum balances are performed. Thus, the governing equations are satisfied exactly at the discrete level. As a result, validity of the solution does not hinge on grid density, although accuracy always does. Due to the inherent nonlinearity in the Navier-Stokes equations, an iterative procedure is used with pressure-velocity coupling handled by the SIMPLE algorithm (Patankar, 1980). This scheme has been applied successfully to many industrial flows and is cited widely in numerous published studies.

Governing equations

The steady three-dimensional equations resulting from the principles of conservation of mass and momentum for an incompressible Newtonian fluid form the basis of the numerical analysis of flow in the U tube. The physical properties are assumed to be constant. The flow is laminar, and the effect of gravity is negligible. With these assumptions, the governing equations for flow in an arbitrary three-dimensional geometry, when written in tensor form, become:

$$\frac{\partial u_i}{\partial x_i}=0 \tag{1}$$

$$u_i \frac{\partial u_j}{\partial x_i}=-\frac{1}{\rho}\frac{\partial p}{\partial x_i}+\frac{\partial}{\partial x_i}\left(\nu \frac{\partial u_j}{\partial x_i}\right) \tag{2}$$

where u_i are the three velocity components, x_i the three coordinate variables, p the pressure, ρ the fluid density, and ν the fluid kinematic viscosity.

Boundary conditions

Because of the elliptic nature of the governing equations, boundary conditions must be specified at all domain boundaries. Four types of boundaries are involved: flow inlets, flow exits, rigid walls, and symmetric planes.

At flow inlets, the flow velocity and all relevant scalar properties must be specified. In this case, a Poiseuille velocity profile is specified at the inlet:

$$u=\frac{2\mu Re}{\rho d}\left(1-\frac{4r^2}{d^2}\right) \quad v=0 \quad w=0 \tag{3}$$

where Re is the inlet Reynolds number based on the tube diameter and inlet average velocity.

At boundaries where flow leaves the domain and the streamwise gradients of the flow field are small, extrapolations may be used because under these conditions, the flow is locally parabolic. This type of boundary condition must be applied carefully, since reflections of the imposed parabolic flow may disturb the flow field upstream. In geometries encountered in this study, care must be exercised to extend the tube sufficiently far away from the bend where the flow is highly elliptic. The extrapolation is described mathematically as:

$$\frac{\partial u}{\partial \vec{n}}=0 \quad \frac{\partial v}{\partial \vec{n}}=0 \quad \frac{\partial w}{\partial \vec{n}}=0 \tag{4}$$

where $\vec{n}$ is the unit normal vector of the outlet plane.

At the solid walls, the usual "no-slip" condition applies:

$$u=0 \quad v=0 \quad w=0 \tag{5}$$

The geometry is symmetric with respect to the plane of the U-tube centerline. Consequently, computational effort can be halved by taking advantage of the symmetry. At the symmetry boundary, the normal velocity and normal gradients of all variables are zero:

$$w=0 \quad \frac{\partial u}{\partial z}=0 \quad \frac{\partial v}{\partial z}=0 \quad \frac{\partial w}{\partial z}=0 \tag{6}$$

where the fact that the symmetry plane is such that $z=0$ has been incorporated in the above definitions.

Numerical method

The numerical solution of the governing partial differential equations (Eqs. 1-2) begins with discretization of the field into a collection of control volumes. The differential equations are approximated by a set of algebraic equations on this collection, and this system of algebraic equations is then solved to produce a set of discrete values which approximate the solution of the partial differential system over the field. First, it is realized that the governing equations can be rewritten in a canonical form as:

$$\frac{\partial}{\partial x_i}(\rho u_i \phi)=\frac{\partial}{\partial x_i}\left(\Gamma \frac{\partial \phi}{\partial x_i}\right)+S \tag{7}$$

where the generic dependent variable ϕ, diffusion coefficient Γ, and source term S can be specified to uniquely define a particular equation. For the mass conservation equations, this set of variables becomes $\phi=1$, $\Gamma=0$, and $S=0$. For the momentum equations, it is $\phi=u_j$, $\Gamma=\mu$, and $S=-\partial p/\partial x_j$.

Discretization. The geometry of the U tube can be described mathematically as a circle sweeping along a curved centerline with the plane of circle always perpendicular to the sweeping direction. For any point on the centerline $(x_o, y_o, 0)$, a local coordinate system $x'y'z'$ is defined such that x' aligns with the flow direction on the centerline. The $x'o'y'$ plane at $z'=0$ is the center plane of the U tube, and the origin is at the point $(x_o, y_o, 0)$. The cross-sectional boundary is defined as:

$$\begin{cases} y'^2+z'^2=R^2 \\ x'=0 \end{cases} \tag{8}$$

Since $z'=z$, the $x'y'z'$ system is related to the xyz coordinates by:

$$\begin{pmatrix} x \\ y \end{pmatrix}=\begin{pmatrix} \cos\alpha & -\sin\alpha \\ \sin\alpha & \cos\alpha \end{pmatrix}\begin{pmatrix} x' \\ y' \end{pmatrix}+\begin{pmatrix} x_o \\ y_o \end{pmatrix} \tag{9}$$

where α is the angle of rotation of the local coordinate system relative to the origin of the system. These relations uniquely define any point on the surface of U tube.

The domain, as defined by the geometry, is discretized into six-sided volume elements which conform to the boundaries. This boundary conforming mesh is created by defining a generalized curvilinear coordinate system which transforms the physical $(x_i,\ i=1,\ 2,\ 3)$ space into a rectangular-shape computational $(\xi^i,\ i=1,\ 2,\ 3)$ space:

$$\xi^i=\xi^i(x_j) \tag{10}$$

These transformation rules must be general enough to accommodate arbitrary geometries. It has been found that the most general method in this respect is to prescribe these rules by solving a set of partial differential equations over the domain of interest as a boundary value problem (Thompson et al., 1985). The Poisson partial differential equations normally used are:

$$\nabla^2 \xi^i(x_j)=P_i(\xi^1,\ \xi^2,\ \xi^3) \tag{11}$$

This transformation introduces a set of contravariant basis vectors:

$$\vec{a}^{\,i}=\nabla \xi^i, \quad i=1,\ 2,\ 3 \tag{12}$$

and a metric tensor and a Jacobian:

$$g^{ij}=g^{ji}=\vec{a}^i\cdot\vec{a}^j, \quad (i=1,\ 2,\ 3) \quad (j=1,\ 2,\ 3) \tag{13}$$

$$\sqrt{g}=\sqrt{\det|g^{ij}|}=[\vec{a}^1\cdot(\vec{a}^2\times\vec{a}^3)]^{-1} \tag{14}$$

In this transformed space, the governing equation (Eq. 7) becomes:

$$\frac{\partial}{\partial \xi^i}(\sqrt{g}u^i\rho\phi)=\frac{\partial}{\partial \xi^i}\left(\sqrt{g}g^{ij}\Gamma\frac{\partial \phi}{\partial \xi^j}\right)+\sqrt{g}S \tag{15}$$

This governing differential equation is rewritten in algebraic forms by performing a surface integral on a typical volume element:

$$\frac{\rho\sqrt{g}(\phi-\phi^o)}{\Delta t}+\sum_{i=1}^{3}(J_i^+-J_i^-)-S\sqrt{g}\prod_{i=1}^{3}\Delta\xi^i=0 \tag{16}$$

where superscript o indicates the previous time step. This form of discretization is fully implicit in time, since all terms except the time derivative are evaluated at the current step. The total

flux (convection and diffusion) through a surface (positive or negative coordinate face) is:

$$J_i = \sqrt{g}u^i\rho\phi - \sqrt{g}g^{ij}\Gamma\frac{\partial\phi}{\partial\xi^j} \tag{17}$$

With the total flux discretized by the power law (Patankar, 1980), the final algebraic form becomes:

$$A_p\phi_p = \Sigma A_{nb}\phi_{nb} + b \tag{18}$$

where subscript p indicates the node point of consideration, and nb for all neighboring points.

Solution Procedures. The algebraic equations derived in the preceding section must be solved systematically. Since the differential equations are nonlinear, the resulting algebraic equations have matrix coefficients that depend on the solution of itself. This dependency calls for an iterative procedure. In addition, the differential equations are coupled, thus the matrix coefficients of one partial differential equation will depend on the solutions of other differential equations as well as itself. Unless the problems involved are small so that all equations can be solved simultaneously, a decoupling on the equation level must be employed. Three-dimensional problems are usually too large to solve all equations simultaneously.

In this study, the algebraic equation system is solved by the algorithm called SIMPLE (Patankar, 1980), a semiimplicit iterative scheme which starts from an initial guess and converges to the correct solution after performing a sufficient number of iterations. Each iteration consists of the following steps:

1. The u, v and w momentum equations are each solved in turn using a guessed pressure field.
2. Since the velocities do not satisfy the mass continuity equation locally, a "Poisson-type" equation is derived from the continuity equation and the linearized momentum equations. This pressure correction equation is then solved to obtain the necessary corrections to the pressure field and corresponding adjustments to the velocity components are made.
3. Scalar transport equations such as those for energy and species are solved using the updated velocity fields.
4. Update all fluid properties.
5. Repeat these steps until the error has decreased to a predetermined tolerance level.

The numerical techniques described thus far are available from a commercial computational fluid dynamics software package (Fluent, 1991a). Customizations were made in the geometry definition, boundary condition specifications, and post-processing routines to fulfill the modeling needs of this research. Validity of the numerical calculations has been verified by several supporting studies (Fluent, 1991b).

The computational grid has $19\times12\times82$ (18,696) volume elements. It is a pseudo-cylindrical type with an artificial radius of 1/40 of the actual tube radius to circumvent the singularity at the tube center which shows up in the figures presented later. All computations were carried out on an HP720 workstation. The tolerance level for convergence was set, as recommended, at 10^{-3} for flow variables. Generally, a solution was obtained within 450 iteration steps in approximately 1.5 CPU hours.

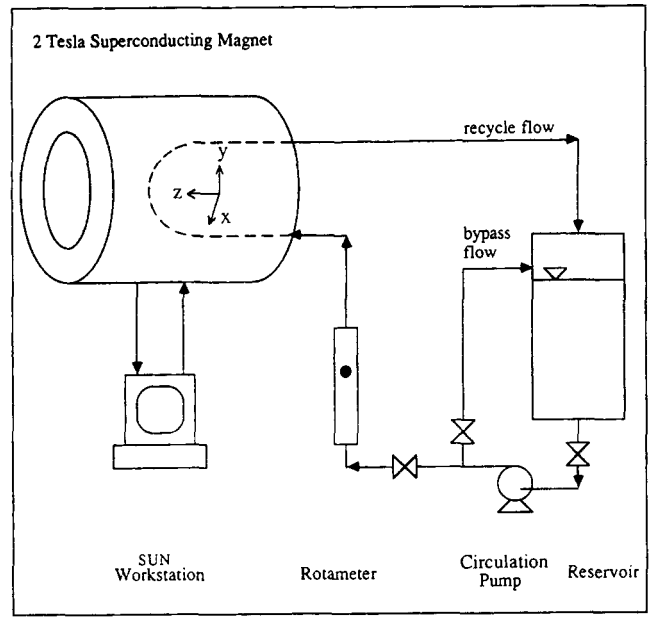

Figure 1a. Flow system for NMR imaging.

Experimental Studies

Flow system

A diagram of the flow system is shown in Figure 1a. Water, doped with 4 g/L copper sulfate ($CuSO_4$) to reduce the relaxation times T_1 and T_2, was pumped (MDR-30T, Eastern/Iwaki Co., CT) from a 45 L reservoir through a rotameter (Model N092-04ST, Cole-Parmer, IL) to the U tube. The glass U tube was placed in a 2 Tesla magnet. The flow was recycled to the reservoir via tygon tubing. The centrifugal pump operated at its maximum flow rate and the flow through the U tube was controlled by valves in the recycle and bypass lines. The temperature was also measured in the bypass line.

A glass U tube with a 180° bend was made as shown in Figure 1b. The longitudinal flow direction is z, and horizontal and vertical directions are x and y, respectively. The U tube is placed horizontally in the magnet (Figure 1a). It has an internal radius of 3.9 mm, 800 mm long and radius of curvature of 25.4 mm, yielding a curvature ratio (tube radius to tube centerline radius) of 0.15.

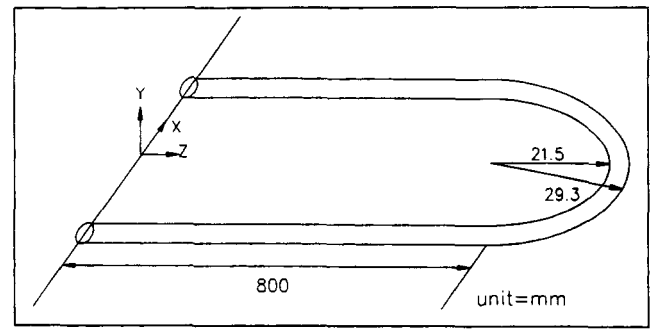

Figure 1b. 180° bend glass U tube.

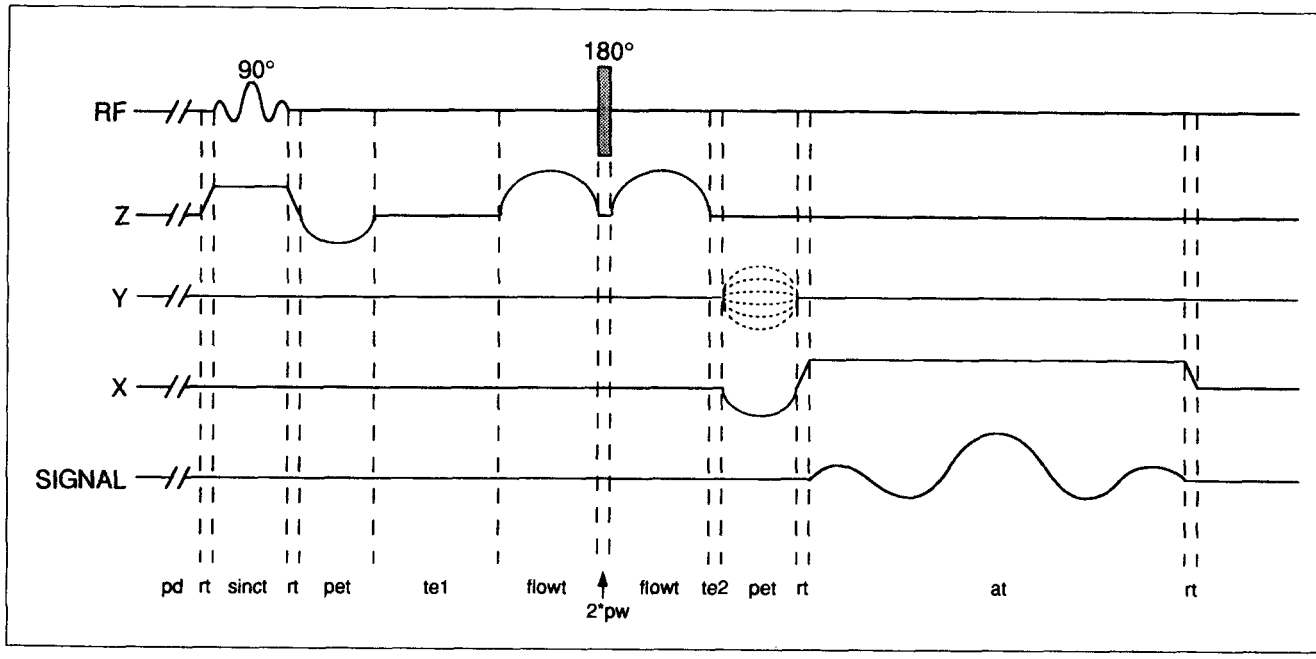

Figure 2. Two-dimensional flow NMR pulse sequence.

See Table 1 for definition and typical values of time intervals.

NMR system and protocol

Flow measurements were conducted with a General Electric, 2 Tesla 310 mm horizontal bore chemical shift imaging (CSI) system at the GE Corporate Research and Development Center in Schenectady, NY. The system was equipped with several sets of strong, self-shielded gradient coils which enabled fast turn-on and turn-off of the gradients. This allowed rapid imaging for flow encoding sequences. A gradient set with a 180 mm bore, 9 G/cm maximum gradient winding with a 5.25 in. (133.35 mm) ID RF coil was used. These high gradients, free of eddy current effects, gave high-quality measurements of velocities and diffusion rates. One image each of flow-on and flow-off was always obtained. Details of the velocity determination are given below.

Flow pulse sequences

Two- and three-dimensional NMR pulse sequences were used to measure flow in the U tube. Figure 2 is a diagram of our two-dimensional flow pulse sequence similar to that described by Dumoulin and Hart (1986) utilizing flow encoding with spin warp imaging (Edelstein et al., 1980). In this case, flow along the z axis is being measured. Flow encoding is accomplished by the two "flow encoding" gradients on either side of the 180° RF refocusing pulse. First, the spins in the sample have their phase shifted by the first gradient during the period "flowt" before the 180° RF pulse. Spins which have not moved have the phase shift undone by the second velocity-encoding lobe in the "flowt" period after the 180° RF pulse. Spins in fluid with a velocity in the z direction will experience a different phase shift in the second gradient lobe than was produced by the first lobe, so their net phase angle differs from the phase angle of spins which did not move.

Table 1. Typical Parameter Values for Acquiring Flow Images

Number of acquisitions, *na*	16
Block size (pixels)	256
Predelay (repetition time), *pd*	150 ms
Echo time (time between 90° RF pulse and center of spin echo)	10 ms
Phase encoding time, *pet*	1 ms
Flow encoding time, *flowt*	1.5 ms
Gradient ramp risetime, *rt*	0.175 ms
First deadtime, *te*1	1.75 ms
Second deadtime, *te*2	0.025 ms
Acquisition time, *at*	5 ms
90° pulse width, *sinct*	1 ms
180° pulse width, 2**pw*	0.15 ms
Slice thickness, *st*	5 mm

This sequence can be used in two ways of measuring flow. One possibility is to apply the pulse sequence to a flowing fluid twice, once with and once without the flow encoding gradients (or with the flow gradients negative, for example). Subtracting the results gives a phase shift of the flowing spins which is a measure of their velocity. Another approach is to apply the sequence to the flowing spins and then to the same sequence with flow switched off. We generally used the latter technique, as we found it produced stabler results in our instrument.

For a constant longitudinal velocity, the phase change ($\Delta\phi$) for a moving spin is proportional to the product of the first moment of the field gradient (G) and the velocity (V) as:

$$\Delta\phi = \gamma V \int tG(t)dt \tag{19}$$

where γ is the gyromagnetic ratio and t is the time.

The other gradients in the sequence are used to obtain spatial information for imaging. First, slice selection is accomplished

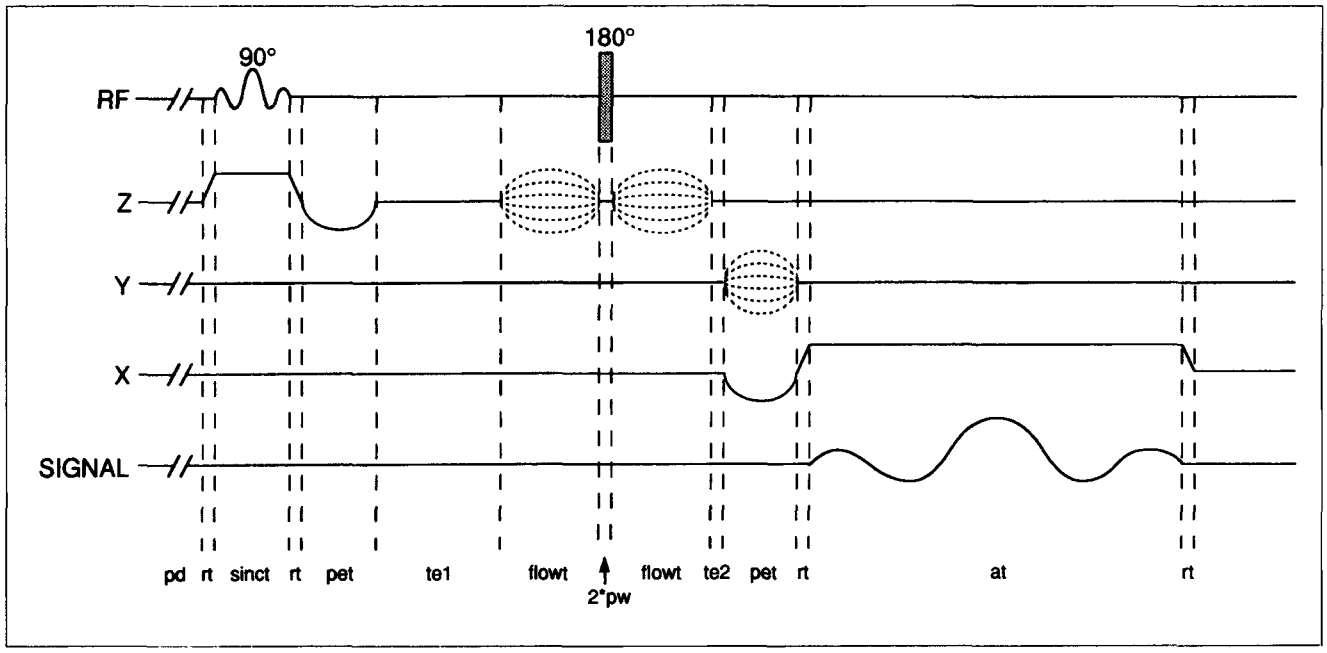

Figure 3. Three-dimensional flow NMR pulse sequence.

See Table 1 for definition and typical values of time intervals.

by applying a 90° RF pulse in the presence of a gradient (interval "sinct"). The figure shows a "sinc" ($sin(x)/x$) shaped pulse which selects an approximately rectangular slice profile for a slice perpendicular to the z axis. During the next interval ("pet") a negative z lobe is applied which refocuses the phases of the spins throughout the slice thickness.

In the interval marked "at," a "readout" gradient is applied along the x axis. This produces a projection of the spatial information onto the x axis. The negative x lobe before the readout gradient for the period "pet" is needed to produce a spin echo in the middle of the "at" period.

A varying set of "phase encoding" gradients is applied along the y axis at the same time as the negative x lobe to obtain spatial information in the y direction.

A three-dimensional pulse sequence in Figure 3 shows that the third dimension represents velocities (Feinberg et al., 1986). The sequence in Figure 3 is similar to the one in Figure 2 except that the flow encoding gradients are varied in steps. When a three-dimensional Fourier transform is applied to data obtained using the pulse sequence of Figure 3, the result is two dimensions of spatial information and one dimension of velocity information.

In our studies, we found that the longitudinal (z direction) velocities could be measured using the two-dimensional flow sequence of Figure 2, but transverse (x and y) velocities could not be reliably detected using the two-dimensional sequence because of their small amplitudes compared to the longitudinal velocity. We could, however, obtain the transverse velocities by using the three-dimensional sequence of Figure 3. Typical parameter values for acquiring flow images are given in Table 1.

NMR flow calibration

To calibrate both the NMR flow measuring methods and the flow system, a flow measurement was made on Poiseuille flow in the curved glass tube placed in the 2 Tesla magnet. Fluid velocities were measured in the straight tubes 400 mm from the curved section using the pulse sequence, as shown in Figure 2.

The mean flow rate was kept constant at $Q = 120$ cm^3/min ($V = 4.2$ cm/s). The phase change $\Delta\phi$ (discussed earlier) for mean longitudinal velocity as a function of magnetic gradient is shown in Figure 4. The phase shift offset vs. gradient was obtained, and the averaged phase shift of the same positive and negative gradients was used to remove this offset, as shown in Figure 5. The theoretical slope obtained from Eq. 19 and

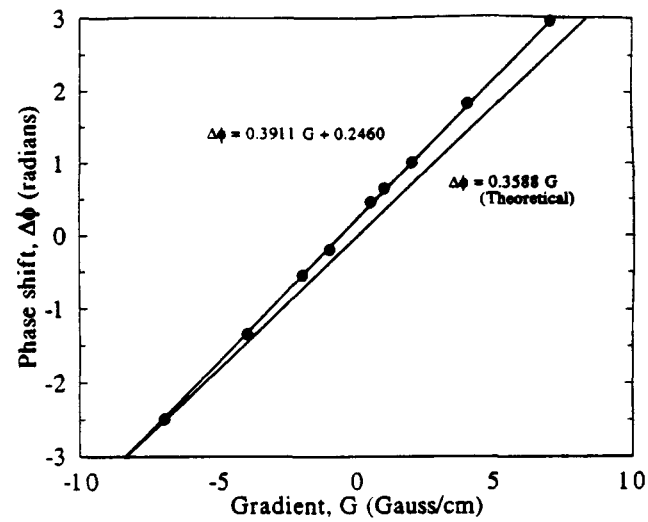

Figure 4. Theoretical vs. experimental phase shift $\Delta\phi$ as a function of flow gradient strength G flow rate $Q = 120$ cm^3/min or average streamwise velocity $V = 4.2$ cm/s.

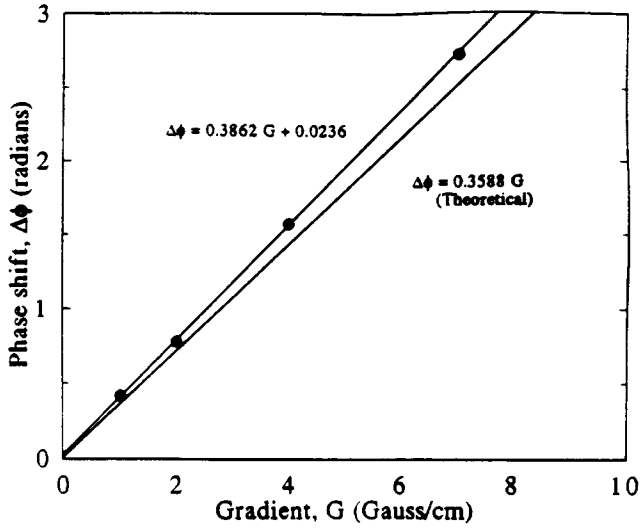

Figure 5. Theoretical vs. averaged experimental phase shift $\Delta\phi$ as a function of flow gradient strength G at a flow rate $Q = 120$ cm^3/min.

the experimental value obtained by NMR agree within 8%. A 5 mm thick slice (z direction) was used, and the parabolic streamwise velocity profile was obtained before and after the U tube far from the curved section, as shown in Figure 6. Errors of the phase map are caused by local variations of the susceptibility and variations of the main flow. We could, however, obtain the transverse velocities by using the three-dimensional sequence of Figure 3. The 2-d sequence (Figure 2) is simpler and easier to implement; the 3-d sequence takes longer to run, but is generally more sensitive and stabler.

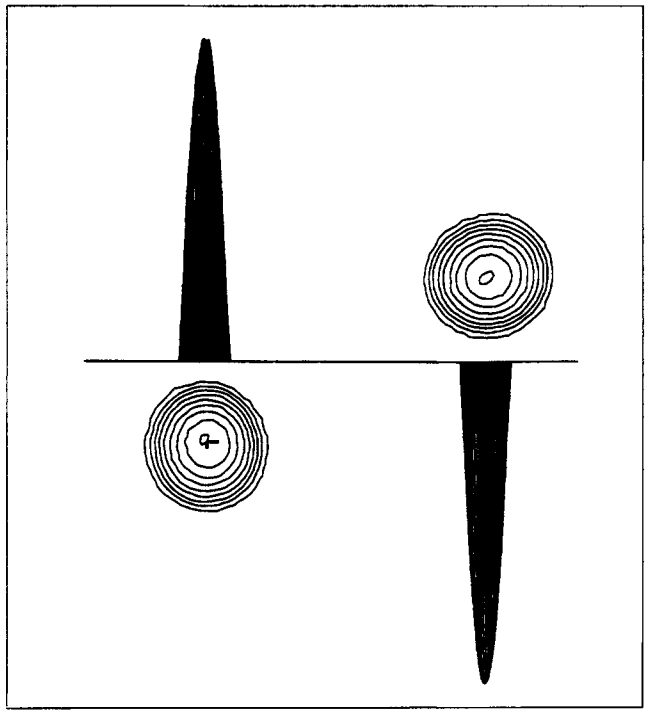

Figure 6. Two-dimensional plots and contours of phase shift magnitude $\Delta\phi$ for flow before and after the U tube far from the curved section at $Q = 120$ cm^3/min.

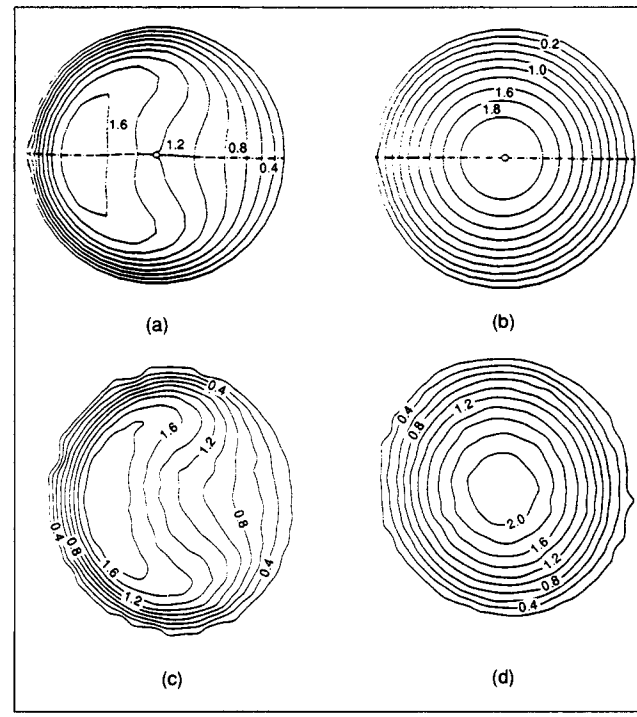

Figure 7. Contours of longitudinal velocities normalized by the average velocity, V, for (a&c) after and (b&d) before the curved section at $Q = 120$ cm^3/min or average streamwise velocity $V = 4.2$ cm/s.

The numerical results are shown above (a&b) and were calculated at the same position (5 mm from the curve) and flow rate as the MRFI results (c&d).

Results and Discussion

Longitudinal velocities near a curve

The longitudinal directional fluid velocity was measured using the two-dimensional pulse sequence shown in Figure 2. The flow rates were kept constant at $Q = 120$, 255 and 315 cm^3/min to within 5%. These correspond to $De = 128$, 272, and 335 for a given curved tube, respectively, where $De = Re\sqrt{(d/2r_c)}$ and $Re = dV/\nu$. A 5.0 mm thick slice (x-y plane) before and after the curved bends (5 mm from the curve) was chosen. Thus, the longitudinal numerical (Figures 7a and 7b) and MRFI (Figures 7c and 7d) velocity contours correspond to flow before and after the 180° curved bend, respectively. The MRFI velocities were taken within 5 mm of the curved bend and normalized by the average streamwise velocity, V. The velocity amplitudes were converted from phase differences $\Delta\phi$ using Eq. 19.

The phase differences were obtained from the flow-on/flow-off data after a two-dimensional Fourier transform to obtain spatial information. Associated with each point in space is a complex number, which is the relative velocity vector. The phase difference $\Delta\phi$ between the flow-on and flow-off vectors

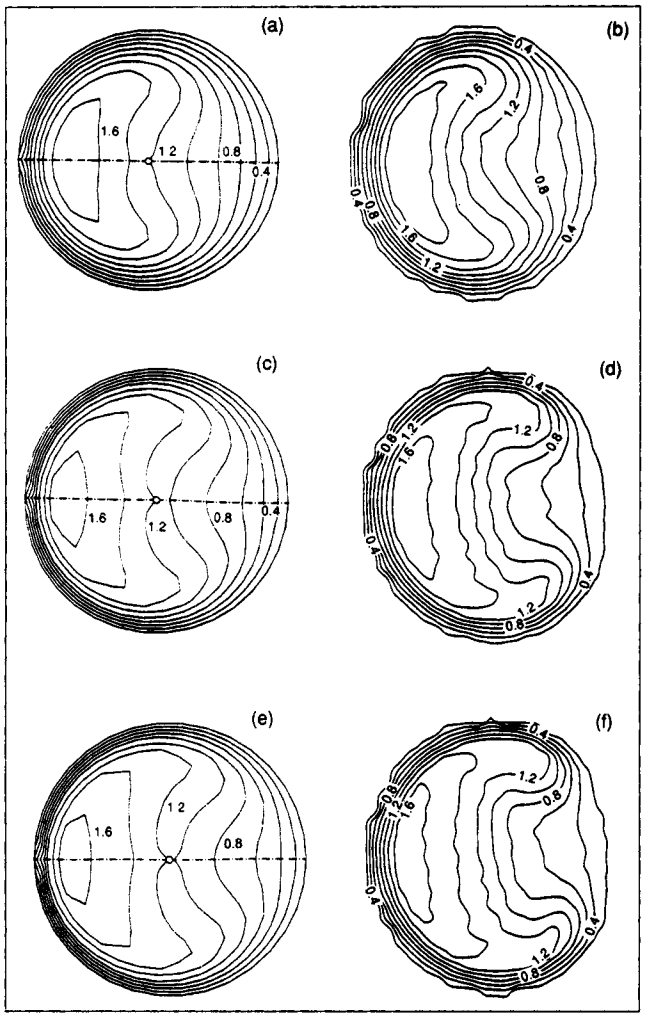

Figure 8. Contours of longitudinal velocities normalized by the average velocity for just after the curved section using 2-d flow sequence (Figure 2) at (a&b) $De = 128$, (c&d) $De = 272$, and (e&f) $De = 335$.

The numerical (a,c&e) and experimental (MRFI) (b,d&f) results are shown on the left and the right, respectively.

can be found from the vector cross product formula: $\vec{a} \times \vec{b} = |\vec{a}| \cdot |\vec{b}| \cdot \sin(\Delta\phi)$. Making the correspondence to complex numbers and solving for $\Delta\phi$, we get:

$$\Delta\phi = \sin^{-1}\left[\frac{\text{Real(flowon)} \cdot \text{Imaginary(flowoff)}}{|\text{flowon}| \cdot |\text{flowoff}|}\right]. \quad (20)$$

The velocity contours before the bend are parabolic profiles (Figures 7b and 7d). However, the local velocity maximum after the bend is offset from the central axis (Figures 7a and 7c). It suggests a convective effect of transverse flows which sweep outward centrally and inward peripherally (Olsen and Snyder, 1985). Also, the formation of crescent-shaped velocity contours toward the outside of the bend is the result of centrifugal force. Note that the shape of the numerical and MRFI contours are similar. The unusual pattern at the center point

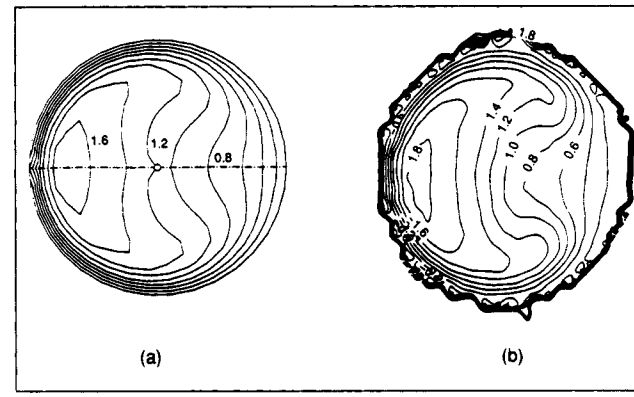

Figure 9. Contours of longitudinal velocities normalized by the average velocity for just after the curved section using 3-d flow sequence (Figure 3) at $De = 272$.

The numerical and experimental (MRFI) results are shown on the left and the right, respectively.

of the numerical plots is due to a singularity and should be ignored. The longitudinal numerical (Figures 8a, 8c and 8e) and MRFI (Figures 8b, 8d and 8f) velocity contours normalized by the average streamwise velocities, V, are $De = 128$, 272, and 335. The position of the maximum velocity and formation of crescent-shaped contours for high Dean number moves progressively toward the outside of the bend. Although not exact, the calculated contours are qualitatively similar to the MRFI measured velocity contours. Also, Olsen and Snyder's (1985) experimental results are similar to air flow in a curved tube for $De = 510$ (not shown), but the maximum velocity is lower

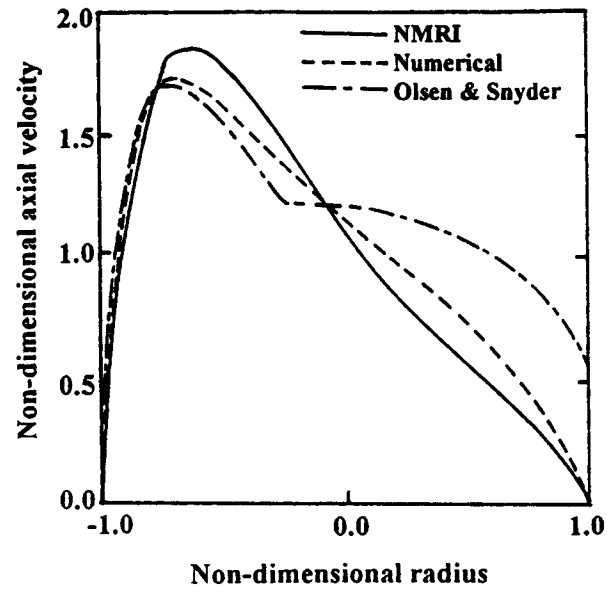

Figure 10. Velocity profiles normalized by the average velocity across the symmetric axis.

The horizontal axis is the nondimensional pipe radius with -1.0 and 1.0 at outer and inner wall of the bend, respectively.

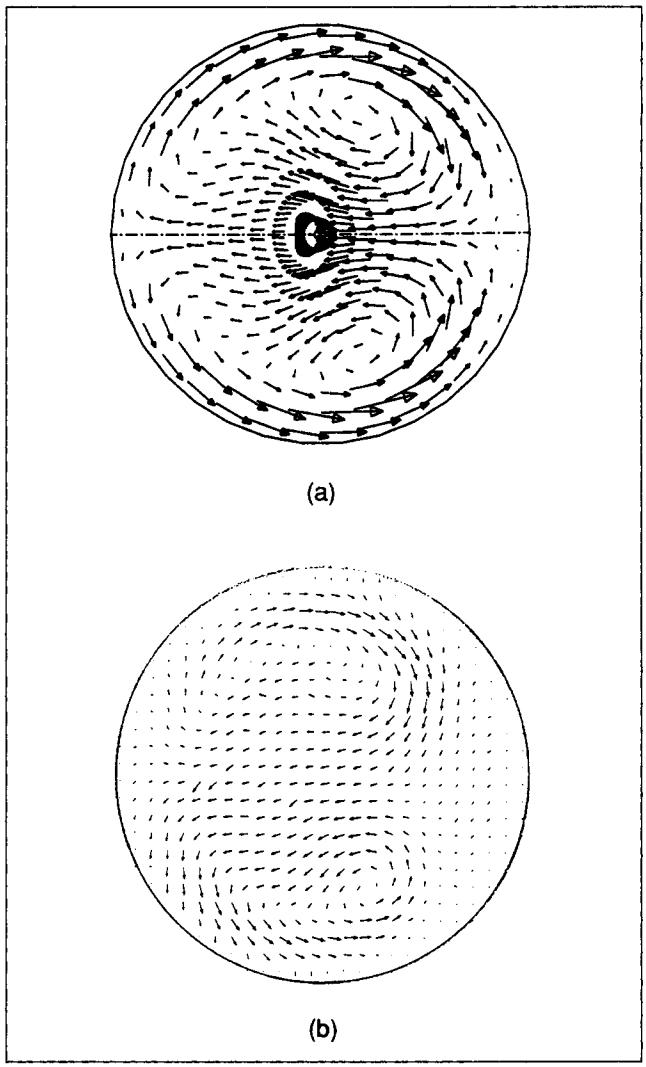

Figure 11. Streamlines of Dean vortex (transversial) flow normalized by the average velocity for just after the curved section using 3-d flow sequence at $De = 272$.

The numerical and experimental (MRFI) results are shown upper (a) and lower (b), respectively.

than that of Olsen and Snyder, because they used a higher centrifugal force (higher Dean number).

The longitudinal MRFI fluid velocity contours for $De = 272$ were also measured using the three-dimensional pulse sequence in Figure 3 and the results are shown in Figure 9. The contours are within 5% of those shown in Figure 8d. Velocity profiles across the symmetric axis are shown in Figure 10. The numerical and experimental (MRFI) results are obtained at $De = 272$ (from Figure 9), but Olsen and Snyder's results (1985) are at $De = 477$.

Transverse velocities near a curve

The x and y (transverse) velocities normalized by the average streamwise velocity, V, for $De = 272$ were measured using the three-dimensional pulse sequence shown in Figure 3. The velocity encoding direction was changed to the GA and GB axes during *flowt* for measuring x- and y-directional velocities, respectively. The transverse velocities combining x- and y-directional velocity are shown in Figure 11. The arrows show the direction of transverse velocities, with relative magnitudes scaled by the arrow lengths. The amplitudes of transverse velocities were one order of magnitude less than the longitudinal velocity. The two-vortex structures in Figure 11 were obtained by numerical (Figure 11a) and MRFI (Figure 11b) methods. Ignoring the singularity at the center of Figure 11a, the numerical result is able to predict the location of the two vortex centers measured by the MRFI technique.

The general direction of the velocity fields are also predicted quite well. However, there are differences probably due to experimental and numerical errors. Since the cross section of the outward flow (along the tube walls and around the vortex eyes) is small relative to the cross section for centrifugal flow across the symmetric axis (centerline), the velocities are higher near the walls than for plane Poiseuille flow, as shown in Figure 11. This may explain why vortices are so efficient in depolarizing and defouling solute from the porous walls of membrane systems.

Conclusions

We report here on a new method, magnetic resonance flow imaging, for measuring velocity contours for curved tube flow. This noninvasive method compliments the LDV and hot wire techniques, both widely used at present. To test these measurements, we compared them with three-dimensional solutions to the velocity field equations using a numerical finite control volume method and data from the literature. In all cases, the comparisons were good.

Acknowledgment

The authors wish to express their appreciation for partial support of this research by Dow Chemical Company, Midland, MI, and their subsidiary, FilmTec Corporation, Minneapolis, MN. Also, they would like to thank Drs. Charles L. Dumoulin, Steven Souza and Peter B. Roemer of General Electric Corporate Research & Development, Schenectady, NY for helpful suggestions and discussions during this work and Dr. Mellisa A. Robinson of the University of Wyoming for help in programming some of the pulse sequences.

Notation

a = contravarient basis vectors
d = tube diameter, cm
De = Dean number $= Re(d/2r_c)^{0.5}$
g = metric tensor
G = field gradient, G/cm
n = normal vector
p = pressure, dyne/cm^2
Q = flow rate, cm^3/min
r = radial coordinate
r_c = mean radius of curvature, cm
Re = Reynolds number $= \rho^* d^* V/\mu$
S = source term (Eq. 7)
t = time, s
T_1 = longitudinal relaxation time, s
T_2 = transverse relaxation time, s
u = velocity in the x direction, cm/s
v = velocity in the y direction, cm/s
V = mean axial velocity, cm/s

w = velocity in the z direction, cm/s
x = coordinate (Eq. 1)
y = coordinate
z = coordinate

Greek letters

α = angle of rotation of the local coordinate system relative to the origin system (Eq. 9)
γ = diffusion coefficient, cm^2/s
Γ = generic diffusion coefficient, cm^2/s or $g/cm \cdot s$
μ = dynamic viscosity (Eq. 7), $g/cm \cdot s$ or gyro magnetic ratio (Eq. 19) $rad/gauss \cdot s$
ν = kinematic viscosity, cm^2/s
ξ = rectangular coordinate (Eq.10)
ρ = fluid density, g/cm^3
ϕ = generic dependent variable (Eq. 7)

Subscripts

i = 1, 2 & 3 for orthogonal coordinates
j = value not equal to i
p = node point under consideration
nb = all neighboring node points

Superscript

$'$ = local coordinates

Literature Cited

Agrawal, Y., L. Talbot, and K. Gong, "Laser Anemometer Study of Flow Development in Curved Circular Pipes," *J. Fluid Mech.*, **85**, 497 (1978).

Akiyama, H., Y. Hanaoki, K. C. Cheng, I. Uroi, and M. Suzuki, "Visual Measurements of Laminar Flow in the Entry Region of a Curved Pipe," *Proc. Int. Symp. on Flow Visualization*, Ann Arbor, W. J. Yang, ed., 526 (1983).

Battocletti, J. H., R. E. Halbach, S. X. Salles-Cunha, and A. Sances, "The NMR Blood Flow-Meter-Theory and History," *Med. Phys.*, **8**, 435 (1981).

Belfort, G., M. E. Brewster, and K. Y. Chung, "Curved Channel Membrane Filtration," U.S. Patent No. 07/903,990 (June 24, 1992).

Berger, S. A., L. Talbot, and L.-S. Yao, "Flow in Curved Tubes," *Ann. Revs. Fluid Mech.*, **15**, 461 (1983).

Bottaro, A., O. J. E. Matsson, and P. H. Alfredsson, "Numerical and Experimental Results for Developing Curved Channel Flow," *Phys. Fluids A*, **3**(6), 1473 (1991).

Bovendeerd, P. H. M., A. A. van Steenhoven, F. N. van de Vosse, and G. Vossers, "Steady Entry Flow in Curved Pipe Flow," *J. Fluid Mech.*, **177**, 233 (1987).

Bradshaw, P., "Turbulent Secondary Flows," *Ann. Rev. Fluid Mech.*, **19**, 53 (1987).

Callaghan, P. T., and Y. Xia, "Velocity and Diffusion Imaging in Dynamic NMR Microscopy," *J. Magn. Reson.*, **91**, 326 (1991).

Caprihan, A., and E. Fukushima, "Flow Measurements by NMR," *Phys. Reports*, **198**(4), 195 (1990).

Choi, U. S., L. Talbot, and I. Cornet, "Experimental Study of Wall Shear Rates in the Entry Region of a Curved Tube," *J. Fluid Mech.*, **93**, 465 (1979).

Chung, K. Y., M. E. Brewster, and G. Belfort, "Dean Vortices with Wall Flux in a Curved Channel Membrane System: 2. The Velocity Field in a Spiral Channel," in preparation (1993a).

Chung, K. Y., M. E. Brewster, and G. Belfort, "Dean Vortices with Wall Flux in a Curved Channel Membrane System: 3. Concentration Polarization in a Spiral Reverse Osmosis Slit," in preparation (1993b).

Chung, K. Y., R. Bates, and G. Belfort, "Dean Vortices with Wall Flux in a Curved Channel Membrane System: 4. Effect of Vortices on Permeation Fluxes of Suspensions in Microporous Membranes," *J. Membrane Sci.*, **81**, 139 (1993c).

Chung, K. Y., W. A. Edelstein, and G. Belfort, "Dean Vortices with Wall Flux in a Curved Channel Membrane System: 6. Two Dimensional Magnetic Resonance Imaging of the Velocity Field in a Curved Impermeable Slit," *J. Membrane Sci.*, **81**, 151 (1993d).

Dean, W. R., "Fluid Motion in a Curved Duct," *Proc. Roy. Soc. A*, **121**, 402 (1928).

Drazin, P. G., and W. H. Reid, *Hydrodynamic Stability*, Cambridge University Press, New York (1981).

Dumouline, C. L., and H. R. Hart, Jr., "Magnetic Resonance Angiography," *Radiology*, **161**, 717 (1986).

Eckmann, D. M., and J. B. Grotberg, "Oscillatory Flow and Mass Transport in a Curved Tube," *J. Fluid Mech.*, **188**, 509 (1988).

Edelstein, W. A., J. M. S. Hutchison, G. Johnson, and T. W. Redpath, "Spin Wrap NMR Imaging and Applications to Human Whole-Body Imaging," *Phys. Med. Biol.*, **25**, 751 (1980).

Enayet, M. M., M. M. Gibson, and A. M. K. P. Taylor, "Laser-Doppler Measurements of Laminar and Turbulent Flow in a Pipe Bend," *Int. J. Heat Fluid Flow*, **3**, 213 (1982).

Feinberg, C. A., L. E. Crooks, P. Sheldon, J. Hoeninger, J. Watts, and M. Arakawa, "Magnetic-Resonance Imaging the Velocity Vector Components of Fluid-Flow," *Magn. Reson. in Med.*, **2**, 555 (1986).

Fluent Inc., *FLUENT User's Manual, Version 3.03*, Lebanon, NH (1991).

Fluent Inc., *FLUENT Version 4 Validation*, Lebanon, NH (1991).

Hammer, B. E., C. A. Heath, S. D. Mirer, and G. Belfort, "Quantitative Flow Measurements in Bioreactors by Nuclear Magnetic Resonance Imaging," *Bio/Technol.*, **8**, 327 (1990).

Hammerlin, D., "Die Stabilitat der Stromung in einem Gekrummten Kanal," *Arch. Rat. Mech. Anal.*, **1**, 212 (1958).

Heath, C. A., G. Belfort, B. E. Hammer, S. D. Mirer, and J. M. Pimbley, "Magnetic Resonance Imaging and Modelling of Flow in Bioreactors by Nuclear Magnetic Resonance Imaging," *AIChE J.*, **36**(4), 547 (1990).

Hemminga, M. A., "Measurement of Flow Characteristics Using Nuclear Magnetic Resonance," *Biomed. Magn. Reson.*, Radiology Research and Education Foundation, San Francisco, p. 157 (1984).

Humphrey, J. A. C., H. Iacovides, and B. E. Launder, "Some Numerical Experiments on Developing Laminar Flow in Circular-Sectioned Bends," *J. Fluid Mech.*, **154**, 357 (1985).

Jones, D. W., and T. F. Child, *Adv. in Magn. Reson.*, **8**, 123, Academic Press, New York (1976).

Kose, K., "NMR Imaging of Turbulent Structure in a Transitional Pipe Flow," *J. Phys. D.: Appl. Phys.*, **23**, 981 (1990).

Kose, K., "One-Shot Velocity Mapping Using Multiple Spin-Echo EPI and Its Application to Turbulent Flow," *J. Magn. Reson.*, **92**, 631 (1991).

Kose, K., "Visualization of Local Shearing Motion in Turbulent Fluids Using Echo-Planar Imaging," *J. Magn. Reson.*, **96**, 596 (1992).

Kroner, K. H., V. Nissinen, and H. Ziegler, "Improved Filtration of Microbial Suspensions," *Bio/Technol.*, **5**, 921 (1987).

Lai, Y. G., R. M. C. So, and H. S. Zhang, "Turbulence-Driven Secondary Flows in a Curved Pipe," *Theoret. Comput. Fluid Dyn.*, **3**, 163 (1991).

Ligrani, P., and R. D. Niver, "Flow Visualization of Dean Vortices in a Curved Channel with 40 to 1 Aspect Ratio," *Phys. Fluids*, **31**(12), 3605 (1988).

Olson, D. E., "Fluid Mechanics Relevant to Respiration: Flow within Curved or Elliptical Tubes and Bifurcating Systems," PhD Thesis, Univ. of London (1971).

Olsen, D. E., and B. Snyder, "The Upstream Scale of Flow Development in Curved Circular Pipes," *J. Fluid Mech.*, **150**, 139 (1985).

Pangrle, B. J., E. G. Walsh, S. C. Moore, and D. DiBiasio, "Magnetic Resonance Imaging of Laminar Flow in Porous Tube and Shell Systems," *Chem. Eng. Sci.*, **47**, 517 (1992).

Patankar, S. V., *Numerical Heat Transfer and Fluid Flow*, Hemisphere, Washington, DC (1980).

Patankar, S. V., V. S. Pratap, and D. B. Spalding, "Prediction of Laminar Flow and Heat Transfer in Helical Coil Pipes," *J. Fluid Mech.*, **62**, 539 (1974).

Reid, W. H., "On the Stability of Viscous Flow in a Curved Channel," *Proc. Roy. Soc. A.*, **244**, 186 (1958).

Singer, J. R., "Blood Flow Rates by Nuclear Magnetic Resonance Measurements," *Sci.*, **130**, 1652 (1959).

Singer, J. R., "NMR Diffusion and Flow Measurements and an Introduction to Spin Phase Graphing," *J. Phys. E: Sci. Instrum.*, **11**, 281 (1978).

So, R. M. C., H. S. Zhang, and Y. G. Lai, "Secondary Cells and Separation in Developing Laminar Curved-Pipe Flows," *Theoret. Comput. Fluid Dyn.*, **3**, 141 (1991).
Soh, W. Y., and S. A. Berger, "Laminar Entrance Flow in a Curved Pipe," *J. Fluid Mech.*, **148**, 109 (1984).
Suryan, J. R., "Nuclear Resonance in Flowing Liquids," *Proc. Indian Acad. Sci.*, **A33**, 107 (1951).
Thompson, J. F., Z. U. A. Warsi, and C. Wayne Mastin, *Numerical Grid Generation: Foundations and Applications*, Elsevier Sci. Publ., New York (1985).
Walowit, J., S. Tsao, and R. DiPrima, "Stability of Flow between Arbitrarily Spaced Concentric Cylinder Surfaces including the Effect of a Radial Temperature Gradient," *J. Appl. Mech.*, **31**, *Trans. ASME*, **86**, 585 (1964).
Xia, Y., P. T. Callaghan, and K. R. Jeffrey, "Imaging Velocity Profiles: Flow through an Abrupt Contraction and Expansion," *AIChE J.*, **38**(9), 1408 (1992).

Manuscript received Nov. 3, 1992, and revision received Mar. 3, 1993.